Adaptive Image-Based Leader–Follower Formation Control of Mobile Robots With Visibility Constraints

Jie Lin, Zhiqiang Miao, *Member, IEEE*, Hang Zhong, Weixing Peng, Yaonan Wang, and Rafael Fierro, *Senior Member, IEEE*

***Abstract*—This article addresses the problem of leader–follower formation control of mobile robots using only onboard monocular cameras that subjected to visibility constraints. An adaptive image-based visual servoing control strategy was proposed following the prescribed performance control methodology. First, the leader–follower visual kinematics in the image plane and an error transformation with predefined performance specifications are presented. Then, an adaptive control law with online estimating the inverse height between the optical center of camera and the single feature point attached to leader is designed to ensure the global stability of the closed-loop system. Finally, the applicability and performance of the proposed control scheme are demonstrated by the numerical simulations and hardware experiments. Compared with other formation control schemes, our solution relies only on onboard visual sensors without communication, since it does not need the relative angle/distance between the robots, or the velocity of the leader. Moreover, it guarantees the prescribed transient and the steady-state performance besides the visibility constraints.**

***Index Terms*—Formation control, mobile robots, prescribed performance, visibility constraints, visual servoing.**

I. Introduction

FORMATION control of multiple mobile robots has been a significant research area in the control and robotics communities thanks to their possible applications in exploration [1], surveillance [2], mapping [3], and transportation [4]. The problem of formation control has been extensively studied, and the formation control strategies mainly fall into four categories: leader–following [5]–[10], behavioral-based [11], [12], virtual structure approaches [13]–[15], and receding horizon control (or model predictive control) [16]–[20]. Each of these approaches has its own advantages and disadvantages, and here we do not intend to provide a completed review on the formation control problem. The reader who is interested in this area is referred to the survey paper [21] for more detailed discussions.

The leader–follower approach is of our particularly interest due to its implementation simplicity and application scalability. However, most of the previous work in leader–follower formation control assume that the global position information of each robot is known and the communication among robots is available. The formation control problem becomes more challenging in GPS-denied and communication-degraded environments. Thus, many solutions have been proposed to expand the application scope and improve the autonomy of robot formations. Compared to other traditional sensors (such as sonar and laser range finder, and LIDAR), the visual cameras can provide richer information at lower cost, making them a very popular option for formation control using only available relative onboard sensing [22].

The various vision-based leader–follower formation control methods can be summarized into two types: position-based visual servoing (PBVS) [23]–[30] and image-based visual servoing (IBVS) [31]–[34]. In the PBVS method, the onboard visual information is used to reconstruct the relative pose between the leader and the followers. The first PBVS approach was proposed in [23], where the controllers were derived from input–output linearization, and the estimators for the relative pose and velocity of the leader were provided by an extended Kalman filter (EKF) based on the measurements from a omnidirectional camera. A Kalman filter was employed in [24] for estimating the position and velocity of leader using vision-based measurements. In [25], the state of the leader–follower system was estimated via the EKF, and the desired formation was stabilized by an estimated state feedback control law. In [26], a method for estimating the relative distance between leader and followers by a reduced-order nonlinear observer was introduced. A geometric pose reconstruction method and a nonlinear velocity estimation strategy were proposed to estimate the relative pose and relative

Manuscript received December 23, 2019; revised April 8, 2020; accepted May 6, 2020. Date of publication May 20, 2020; date of current version March 22, 2021. This work was supported in part by the National Key R&D Program of China under Grant 2018YFB1308200, in part by the National Natural Science Foundation of China under Grant 61903135, Grant 61803089, and Grant 61733004, in part by the Key R&D Program of Hunan Province under Grant 2018GK2022, and in part by the Fundamental Research Funds for the Central Universities under Grant 531118010224. *(Corresponding author: Zhiqiang Miao.)*

Jie Lin, Zhiqiang Miao, Hang Zhong, Weixing Peng, and Yaonan Wang are with the College of Electrical and Information Engineering, and the National Engineering Laboratory for Robot Visual Perception and Control, Hunan University, Changsha 410082, China (e-mail: linjie0275@hnu.edu.cn; miaozhiqiang@hnu.edu.cn; zhonghang@hnu.edu.cn; weixing_peng@hnu.edu.cn; yaonan@hnu.edu.cn).

Rafael Fierro is with the MARHES Lab, Department of Electrical and Computer Engineering, University of New Mexico, Albuquerque, NM 87131-0001 USA (e-mail: rfierro@unm.edu).

Color versions of one or more of the figures in this article are available online at https://ieeexplore.ieee.org.

Digital Object Identifier 10.1109/TIE.2020.2994861

speed between robots in [27]. In [28], a controller that does not need to measure the leader's velocity was proposed based on the relative pose reconstructed from the homography relations and a known fiducial geometry. A method for estimating the relative distance based on the height information of the robot and the cylinder was proposed in [29], and the cohesive movement of the autonomous formation was realized by decentralized control laws. A leader and follower relative position observer was developed in [30] by integrating feedback from monocular cameras, odometers, and AHRS sensors. Compared to PBVS, the IBVS method achieves the tracking of the desired pose of the leader by directly controlling the error of the current image coordinates and the desired image coordinates. Therefore, the IBVS method is more preferred for the formation control of mobile robots because it is less sensitive to camera calibration and object model errors. In [31], a nonlinear controller in the image plane was presented for nonholonomic robots equipped with central panoramic cameras. A new active vision-based formation system using a pan-controlled camera without inter-robot range estimation and communication was proposed in [32]. A real-time observer was proposed in [33] to accommodate the unknown internal and external parameters of the monocular camera. In [34], an adaptive formation control law was developed in image space without leader's position and velocity measurements.

The main concern on the aforementioned studies is that omnidirectional (or pan-controlled) cameras are used. However, the onboard cameras inherently have limited field of view, which impose additional visibility constraints on the motion of the system. The visibility constraints, therefore, should be taken into account when designing the formation control algorithms. In [35], the visibility constraints were characterized by a convex and polyhedral set encoding both the position and angular information, and then a solution was introduced based on the conception of controlled invariance. By modeling the limited sensing region as a cone of view, a vision-based formation control strategy was proposed in [36], where the visibility maintenance and formation were respectively guaranteed based on set-theoretic methods and dipolar vector fields. In [37], the visibility constraints also were modeled as a cone of view of Kinect, and then were converted into input constraints. The proposed formation controller therein was compensated by an auxiliary design system to ensure formation keeping under visibility maintenance. In [38], a decentralized control protocol was proposed for vehicular platoons with cameras that have limited range and angle of view. It should be noted that the visibility constraints in the aforementioned studies all are imposed on metrics in the configuration space (position and orientation in [35], distance and bearing in [36]–[38]). Thus, they belong to the PBVS solutions since pose reconstruction is still necessary when addressing the visibility constraints.

In this article, we intend to solve the problem of vision-based leader–follower formation control without violating the visibility constraints exclusively in the image space. Using the prescribed performance control technology [39]–[42], a new IBVS formation control scheme is proposed to achieve predefined performance specifications and satisfy the field of view constraints. Note that the barrier Lyapunov function and potential function-based methods can also handle state constraints. Generally, they mainly prevent the constrained states from the bounds, and thus, stay within the interior of a feasible or safe area. Compared with the barrier or potential function-based methods, the prescribed performance control methods can regulate the control error to a predefined residual set that is bounded by an absolutely decaying function of time. As a result, the prescribed performance-based controller not only ensures the visibility constraints, but also guarantees transient and the steady-state performance. Specifically, the proposed controller consists of a simple visual feedback control law and an online parameter adaptive law. The feedback control law relies only on the image errors, and the adaptive law aims to estimate the relative height between the optical center of camera onboard the follower and the single feature point attached to leader. Using the Lyapunov stability analysis, global stability and, thus, the prescribed performance of the formation error system can be guaranteed. Compared with other vision-based formation control schemes, the main contributions of this article can be summarized as follows.

1) Our solution requires minimal sensing capabilities, since it relies only on one monocular camera onboard the follower and one feature point attached to the leader. In contrast, omnidirectional cameras were adopted in [31], and active pan-controlled cameras were used in [32].
2) The proposed controller is of considerably low computational complexity. It involves very few and simple calculations, and does not need to estimate the relative position, the relative angle between the leader and the follower, or the velocity of the leader. While in [33], a relatively complex and dynamic controller along with an image-based filter and a nonlinear observer were proposed. In [34], the velocity of the leader has to be estimated online, and the relative angle was computed using the homography-based technique.
3) Compared with solutions in [35]–[38], the visibility constraints are addressed directly in the image space. By selecting performance functions appropriately, the proposed strategy ensures that the image coordinate errors converge under the specified transient and steady-state performance indicators without violating the visibility constraints.

The remainder of this article is organized as follows. Section II presents the system modeling and the problem statement. In Section III, the control design and the corresponding stability analysis are given. Simulation and experimental results for illustrating the effectiveness of the proposed control approach are provided in Section IV. Section V concludes this article. A flowchart shown in Fig. 1 gives the global view of the proposed methodology.

II. Problem Formulation

A. Leader–Follower Kinematics

The basic leader–follower setup considered here is shown in Fig. 2. It contains a leader robot R_l and a follower R_f moving

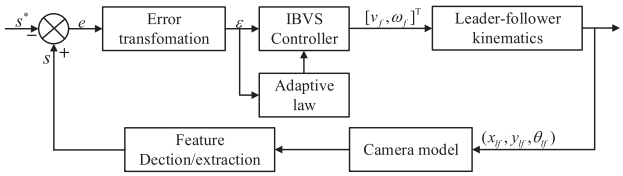

Fig. 1. Diagram of the proposed control scheme.

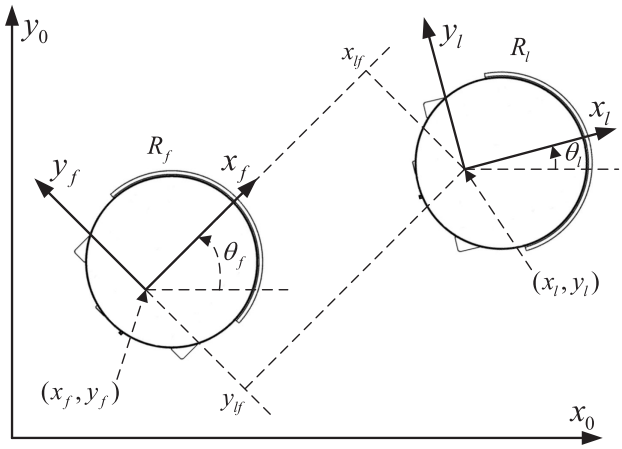

Fig. 2. Leader–follower setup in configuration space.

on a plane. When the mobile robots satisfy the "pure rolling and nonslipping" nonholonomic constraints, the kinematics of each robot can be described by

$$\begin{aligned}\dot{x}_i &= v_i \cos\theta_i \\ \dot{y}_i &= v_i \sin\theta_i \\ \dot{\theta}_i &= \omega_i\end{aligned} \tag{1}$$

where $i \in \{l, f\}$, $r_i = [x_i, y_i]^T$ and θ_i are, respectively, the position and orientation of robot R_i with respect to the world reference system $\mathcal{F}_0$; and v_i and ω_i are the linear velocity and angular velocity of robot R_i in the body-fixed frame $\mathcal{F}_i$.

Define the position $r_{lf} = [x_{lf}, y_{lf}]^T$ of the leader with respect to the follower frame as:

$$r_{lf} = R(\theta_f)(r_l - r_f) \tag{2}$$

where $R(\theta_f)$ is a rotation matrix defined by

$$R(\theta_f) = \begin{bmatrix} \cos\theta_f & \sin\theta_f \\ -\sin\theta_f & \cos\theta_f \end{bmatrix}.$$

Taking the time derivative of r_{lf}, one get

$$\dot{r}_{lf} = \begin{bmatrix} 0 & \omega \\ -\omega & 0 \end{bmatrix} r_{lf} + \begin{bmatrix} \cos\theta_{lf} \\ \sin\theta_{lf} \end{bmatrix} v_l - \begin{bmatrix} 1 \\ 0 \end{bmatrix} v_f \tag{3}$$

where $\theta_{lf} = \theta_l - \theta_f$ is the relative angle between R_l and R_f that satisfies

$$\dot{\theta}_{lf} = \omega_l - \omega_f. \tag{4}$$

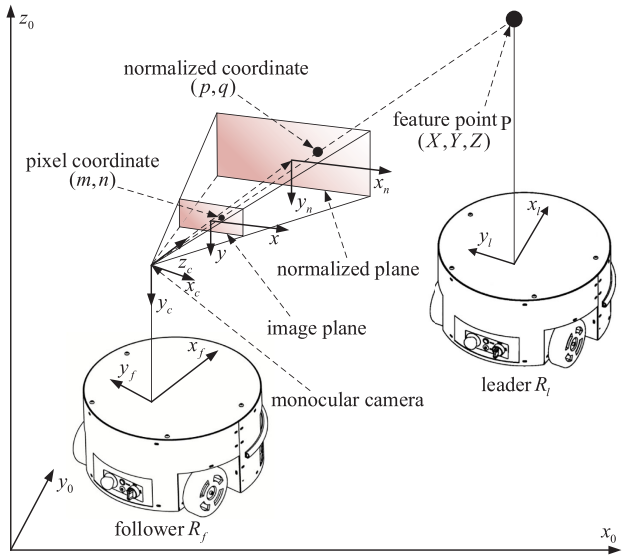

Fig. 3. Camera setup for the leader–follower system.

Combining (3) and (4), the leader–follower kinematics in configuration space is obtained as follows:

$$\begin{aligned}\dot{x}_{lf} &= \omega_f y_{lf} + v_l \cos\theta_{lf} - v_f \\ \dot{y}_{lf} &= -\omega_f x_{lf} + v_l \sin\theta_{lf} \\ \dot{\theta}_{lf} &= \omega_l - \omega_f.\end{aligned} \tag{5}$$

B. Camera Model and Visibility Constraints

Here, a camera is utilized in the leader–following system to obtain the information required to coordinate their motion. As shown in Fig. 3, we assume that a monocular camera is mounted onboard the follower robot with the optical axis is aligned with the x-axis of frame $\mathcal{F}_f$. Using the common pinhole camera model, the relationship between a 3-D point with coordinate $P = [X, Y, Z]^T$ in the camera frame, and its corresponding 2-D point in the image plane with coordinate $u = [m, n]^T$ is given by

$$m = \alpha_m \frac{X}{Z} + m_0,\ n = \alpha_n \frac{Y}{Z} + n_0 \tag{6}$$

where $\alpha_m > 0$ and $\alpha_n > 0$ are, respectively, the scaling factors in the horizontal and vertical directions, (m_0, n_0) denote the image coordinate of the cameras principal point.

Since the onboard camera has limited capabilities, the feature point is visible to it only when the feature point stays within its field of view. The image coordinates of the feature point are subjected to the following visibility constraints:

$$m_{\min} \le m \le m_{\max},\ n_{\min} \le n \le n_{\max} \tag{7}$$

where $m_{\min}$, $n_{\min}$ and $m_{\max}$, $n_{\max}$ denote the minimum and maximum values of the image coordinates m, n, respectively.

To facilitate the following control development, we define the normalized coordinates $s = [p,\ q]^T$ as

$$p = \frac{X}{Z} = \frac{m - m_0}{\alpha_m},\ q = \frac{Y}{Z} = \frac{n - n_0}{\alpha_n} \tag{8}$$

and the corresponding constraints imposed on the normalized coordinates are

$$p_{\min} \le p \le p_{\max},\ q_{\min} \le q \le q_{\max} \tag{9}$$

where $p_{\min}, p_{\max}$ and $q_{\min}, q_{\max}$ can be obtained as

$$p_{\min} = \frac{m_{\min} - m_0}{\alpha_m},\ p_{\max} = \frac{m_{\max} - m_0}{\alpha_m}$$
$$q_{\min} = \frac{n_{\min} - n_0}{\alpha_n},\ q_{\max} = \frac{n_{\max} - n_0}{\alpha_n}.$$

C. Problem Statement

This article intends to propose a visual feedback controller for the leader–following system using only information from onboard camera images. Specifically, given a desired constant visual feature vector $s^* = [p^*, q^*]^T$, the goal is to design a controller for the follower robot so that the visual feature converges to a predefined and arbitrarily small neighborhood of s^* without violating the visibility constraints.

The following assumptions are necessary to design the formation controller.

Assumption 1: The velocity of leader cannot be measured, but it is bounded.

Assumption 2: The feature point P is initially within the field-of-view of camera.

III. IBVS Control Design

A. Visual Kinematics

In this section, the relative kinematics between the leader and the follower in the image space is derived. The kinematic system model (5) in configuration space is incorporated with the camera measurement model. Suppose that the optical center of the camera lies on the z-axis of the follower frame, and the feature point lies on the z-axis of the leader frame. Thus, the position of the feature point with respect to the camera frame can be obtained as

$$[X, Y, Z]^T = [-y_{lf}, h, x_{lf}]^T \tag{10}$$

where the constant h is the relative height between the optical center of the camera and the feature point. Using (5), then the kinematics of the feature point in the camera frame is given by

$$\begin{aligned} \dot{X} &= \omega_f Z - v_l \sin\theta_{lf} \\ \dot{Y} &= 0 \\ \dot{Z} &= -\omega_f X + v_l \cos\theta_{lf} - v_f. \end{aligned} \tag{11}$$

Taking the time derivative of (8) yields

$$\dot{p} = \frac{\dot{X}}{Z} - p\frac{\dot{Z}}{Z},\ \dot{q} = \frac{\dot{Y}}{Z} - q\frac{\dot{Z}}{Z}. \tag{12}$$

After substituting (11) into (12), and using the fact that

$$Z = h/q \tag{13}$$

then the open-loop visual kinematics in terms of the linear and angular velocities in the normalized image space is given by

$$\begin{aligned} \begin{bmatrix} \dot{p} \\ \dot{q} \end{bmatrix} &= \begin{bmatrix} \frac{1}{h}pq & 1+p^2 \\ \frac{1}{h}q^2 & pq \end{bmatrix} \begin{bmatrix} v_f \\ \omega_f \end{bmatrix} \\ &\quad + \frac{1}{h}\begin{bmatrix} -q\sin\theta_{lf} - pq\cos\theta_{lf} \\ -q^2\cos\theta_{lf} \end{bmatrix} v_l. \end{aligned} \tag{14}$$

Generally, the relative height parameter h is unknown. To make the problem solvable, it is reasonable to assume the following.

Assumption 3: The parameter $h \neq 0$, the sign of h is known, and there exists positive constants $\underline{h} > 0,\ \overline{h} > 0$, such that $\underline{h} \le |h| \le \overline{h}$.

B. Prescribed Performance Control

Based on the visual kinematics developed in the previous section, the prescribed performance control technique is utilized here to achieve predefined dynamic and steady-state response for image coordinate errors, as well as satisfy the visibility constraints.

First define the image error $e = [e_1, e_2]^T$ with

$$e_1 = p - p^*,\ e_2 = q - q^*. \tag{15}$$

A controller achieves the prescribed performance when the image errors e_1 and e_2 converge to a predefined residual set that is bounded by absolutely decaying function of time. Typically, the prescribed performance can be mathematically expressed by the following inequalities:

$$-\underline{C}_k \rho_k(t) < e_k < \overline{C}_k \rho_k(t) \tag{16}$$

where $k = \{1, 2\}$, $\underline{C}_k$ and $\overline{C}_k$ are positive parameters, and the performance function $\rho_k(t)$ is defined by

$$\rho_k(t) = \left(1 - \frac{\rho_\infty}{\max\{\underline{C}_k, \overline{C}_k\}}\right) e^{-lt} + \frac{\rho_\infty}{\max\{\underline{C}_k, \overline{C}_k\}} \tag{17}$$

where the constant $l > 0$ denotes the convergence rate of the tracking error, and $\rho_\infty > 0$ represents the steady-state performance specification, which can be set small enough to meet performance requirements. To ensure the field of view constraints, we select

$$\underline{C}_1 = p^* - p_{\min},\ \overline{C}_1 = p_{\max} - p^* \tag{18}$$

$$\underline{C}_2 = q^* - q_{\min},\ \overline{C}_2 = q_{\max} - q^*. \tag{19}$$

Because $0 < \rho_k(t) < 1$ for all $t > 0$, under Assumption 2, one can obtain $p_{\min} < p(t) < p_{\max},\ q_{\min} < q(t) < q_{\max}$ for all $t > 0$, which implies the visibility constraints can be always satisfied.

To achieve formation control with prescribed performance (16), an error transformation first is introduced. The transformation function $T(\varepsilon_k)$ is defined such that

$$e_k = T(\varepsilon_k)\rho_k(t) \tag{20}$$

where function $T(\varepsilon_k)$ is strictly increasing and satisfies the following requirements:

$$\begin{cases} -\underline{C}_k < T(\varepsilon_k) < \overline{C}_k \\ \lim\limits_{\varepsilon_k \to +\infty} T(\varepsilon_k) = \overline{C}_k \\ \lim\limits_{\varepsilon_k \to -\infty} T(\varepsilon_k) = -\underline{C}_k \end{cases}.$$

According to the abovementioned requirements, the error transformation function $T(\varepsilon_k)$ can be chosen as

$$T(\varepsilon_k) = \frac{e^{\varepsilon_k}\overline{C}_k - \underline{C}_k}{e^{\varepsilon_k} + 1}. \tag{21}$$

Since $T(\varepsilon_k)$ is strictly increasing, its inverse function always exists. If we denote $\xi_k = e_k/\rho_k$, then the inverse function can be described by

$$\varepsilon_k = \ln\left(\frac{\xi_k + \underline{C}_k}{\overline{C}_k - \xi_k}\right). \tag{22}$$

In what follows, the system model on the unconstrained error is considered. First, we rewrite (14) in a more compact form

$$\dot{e} = G[\lambda v_f, \omega_f]^{\mathrm{T}} + \lambda f v_l \tag{23}$$

where $\lambda = 1/h$, and the matrix G and vector f are given by

$$G = \begin{bmatrix} pq & 1+p^2 \\ q^2 & pq \end{bmatrix},\ f = \begin{bmatrix} -q\sin\theta_{lf} - pq\cos\theta_{lf} \\ -q^2\cos\theta_{lf} \end{bmatrix}.$$

Then, the time derivative of transformed error gives

$$\dot{\varepsilon} = J\left(G[\lambda v_f, \omega_f]^{\mathrm{T}} + \lambda f v_l + \delta\right) \tag{24}$$

where $J = \mathrm{diag}(J_1, J_2)$ and $\delta = [\delta_1, \delta_2]^T$ are defined as

$$J_k = \frac{\partial \varepsilon_k}{\partial e_k} = \frac{\overline{C}_k - \underline{C}_k}{(\xi_k + \underline{C}_k)(\overline{C}_k - \xi_k)\rho_k}$$

$$\delta_k = \frac{\partial \varepsilon_k}{\partial t} = -\dot{\rho}_k \xi_k.$$

Now we are ready to design the control law for system (24) with unknown parameter λ. Denote $\hat{\lambda}$ as the estimation of λ, and consider the adaptive control law as follows:

$$[v_f, \omega_f]^{\mathrm{T}} = [\bar{v}_f/\hat{\lambda}, \bar{\omega}_f]^{\mathrm{T}} \tag{25}$$

$$[\bar{v}_f, \bar{\omega}_f]^{\mathrm{T}} = -G^{-1}\left[(J^{-1}K_1 + K_2 J^T)\varepsilon\right] \tag{26}$$

where K_1 and K_2 are positive definite matrices, and $\hat{\lambda}$ is online tuned by the following adaptive law:

$$\dot{\hat{\lambda}} = \begin{cases} \gamma \varepsilon^{\mathrm{T}} J g v_f & \text{if } 1/\overline{h} < \mathrm{sgn}(h)\hat{\lambda} < 1/\underline{h} \\ & \text{or } \mathrm{sgn}(h)\hat{\lambda} = 1/\overline{h} \ \&\ \mathrm{sgn}(h)\varepsilon^{\mathrm{T}} J g v_f \geq 0 \\ & \text{or } \mathrm{sgn}(h)\hat{\lambda} = 1/\underline{h} \ \&\ \mathrm{sgn}(h)\varepsilon^{\mathrm{T}} J g v_f \leq 0 \\ 0 & \text{otherwise} \end{cases} \tag{27}$$

where $\gamma > 0$ is a positive gain, and the vector $g = [pq,\ q^2]^T$. Assume that the initial condition $\hat{\lambda}(0)$ satisfies $1/\overline{h} \leq \mathrm{sgn}(h)\hat{\lambda}(0) \leq 1/\underline{h}$.

C. Stability Analysis

Under the proposed adaptive control law, the corresponding stability results on system (24) can be stated in the following claim.

Theorem 1: Consider system (14) with the adaptive control law presented by equations (25)–(27), then the error system (24) is stable, all the closed-loop signals are uniformly ultimately bounded, and the prescribed performance (16) is guaranteed.

Proof: Substituting (25) and (26) into (24), then the error system becomes

$$\begin{aligned} \dot{\varepsilon} = &\ JG[\bar{v}_f, \bar{\omega}_f]^{\mathrm{T}} + JG[\tilde{\lambda} v_f, 0]^{\mathrm{T}} + J(\lambda f v_l + \delta) \\ = &\ -K_1\varepsilon - JK_2J^T\varepsilon + \tilde{\lambda} J g v_f + J(\lambda f v_l + \delta) \end{aligned} \tag{28}$$

where $\tilde{\lambda} = \lambda - \hat{\lambda}$. Consider the following Lyapunov candidate

$$V = \frac{1}{2}\varepsilon^T\varepsilon + \frac{1}{2\gamma}\tilde{\lambda}^2 \tag{29}$$

then the time derivative of V is

$$\begin{aligned} \dot{V} = &\ -\varepsilon^T K_1 \varepsilon - \varepsilon^T JK_2J^T\varepsilon + \varepsilon^T J(\lambda f v_l + \delta) \\ &+ (\gamma \varepsilon^T J g v_f - \dot{\hat{\lambda}})\tilde{\lambda}/\gamma. \end{aligned} \tag{30}$$

Under the adaptive law (27), it can be easily proved that $1/\overline{h} \leq \mathrm{sgn}(h)\hat{\lambda}(t) \leq 1/\underline{h}$ always holds provided that $1/\overline{h} \leq \mathrm{sgn}(h)\hat{\lambda}(0) \leq 1/\underline{h}$. Furthermore, if $\mathrm{sgn}(h)\hat{\lambda} = 1/\overline{h}$ and $\mathrm{sgn}(h)\varepsilon^{\mathrm{T}} J g v_f < 0$, then $(\gamma\varepsilon^T J g v_f - \dot{\hat{\lambda}})\tilde{\lambda} = \gamma\varepsilon^T J g v_f \tilde{\lambda} = \gamma\varepsilon^T J g v_f(1/h - \hat{\lambda}) = \mathrm{sgn}(h)\gamma\varepsilon^T J g v_f(1/|h| - 1/\overline{h}) \leq 0$. If $\mathrm{sgn}(h)\hat{\lambda} = 1/\underline{h}$ and $\mathrm{sgn}(h)\varepsilon^{\mathrm{T}} J g v_f > 0$, then $(\gamma\varepsilon^T J g v_f - \dot{\hat{\lambda}})\tilde{\lambda} = \gamma\varepsilon^T J g v_f \tilde{\lambda} = \gamma\varepsilon^T J g v_f(1/h - \hat{\lambda}) = \mathrm{sgn}(h)\gamma\varepsilon^T J g v_f(1/|h| - 1/\underline{h}) \leq 0$. Otherwise, $(\gamma\varepsilon^T J g v_f - \dot{\hat{\lambda}})\tilde{\lambda} = 0$. Thus, (30) gives

$$\dot{V} \leq -\varepsilon^T K_1 \varepsilon - \varepsilon^T JK_2J^T\varepsilon + \varepsilon^T J(\lambda f v_l + \delta). \tag{31}$$

Using the Young's inequality, one get

$$\varepsilon^T J(\lambda f v_l + \delta) \leq \sigma\|J^T\varepsilon\|^2 + \frac{1}{4\sigma}\|\lambda f v_l + \delta\|^2 \tag{32}$$

where constant $\sigma > 0$. Because $\delta_k = -\dot{\rho}_k\xi_k = -\dot{\rho}_k T(\varepsilon_k)$, $T(\varepsilon_k)$, and $\dot{\rho}_k$ are bounded, $\|\delta\|$ is bounded. Since $|p| = |e_1 + p^*| \leq |T(\varepsilon_1)\rho_1(t)| + |p^*| \leq |T(\varepsilon_1)| + |p^*|$, and $|q| = |e_2 + q^*| \leq |T(\varepsilon_2)\rho_2(t)| + |q^*| \leq |T(\varepsilon_2)| + |q^*|$, it can be concluded that p and q, and hence, $||g||$ are bounded. Thus, there exists a constant $\Delta > 0$ such that

$$\|\lambda f v_l + \delta\| \leq |\lambda v_l|\|f\| + \|\delta\| \leq \Delta \tag{33}$$

which implies that

$$\begin{aligned} \dot{V} &\leq -\varepsilon^T K_1\varepsilon - \varepsilon^T JK_2J^T\varepsilon + \sigma\|J^T\varepsilon\|^2 + \frac{\Delta^2}{4\sigma} \\ &\leq -\varepsilon^T K_1\varepsilon - (\lambda_{\min}(K_2) - \sigma)\|J^T\varepsilon\|^2 + \frac{\Delta^2}{4\sigma} \end{aligned} \tag{34}$$

where $\lambda_{\min}(K_2) > 0$ is the minimum eigenvalue of matrix K_2. We assume that K_2 and σ are chosen such that $\lambda_{\min}(K_2) \geq \sigma$, then (34) can be rewritten as

$$\dot{V} \leq -cV + b \tag{35}$$

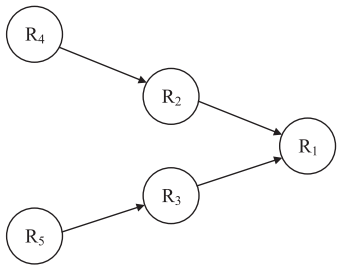

Fig. 4. Leader–follower formation topology in the simulation: Robot R_1 is the group leader, robots R_2 and R_3 are the followers of robot R_1, while robots R_4 and R_5 are, respectively, the followers of robots R_2 and R_3.

where $c = 2\lambda_{\min}(K_1) > 0$, and $b = \Delta^2/4\sigma + \lambda_{\min}(K_1)(\overline{h} - \underline{h})^2/(\gamma \overline{h}^2 \underline{h}^2)$. Using the Lyapunov stability theory, it can be concluded that the closed-loop system is stable, and all the signals are uniformly ultimately bounded. Since ε is bounded, and using the properties of function $T(\varepsilon)$, one get $-\underline{C}_k < T(\varepsilon_k) < \overline{C}_k$. Hence $-\underline{C}_k \rho_k(t) < e_k(t) < \overline{C}_k(t)\rho_k(t)$, which implies the prescribed error performance (16) and consequently the visibility constraints can be guaranteed. ■

IV. Simulation and Experimental Results

A. Simulation Results

This section presents some simulations to verify the validity and performance of the proposed leader–follower formation control scheme. By default, the values of variables are in SI units. In the simulation, we consider a group of five nonholonomic mobile robots $R_1 - R_5$, whose leader–follower interactive topology is shown in Fig. 4. The relative heights between the camera onboard R_i and the feature point on R_j, respectively, are assumed to be $h_{12} = h_{13} = -0.27, h_{24} = h_{35} = 0.27$ (or $\lambda_{12} = \lambda_{13} = -3.7, \lambda_{24} = \lambda_{35} = 3.7$). The designed control algorithm is simulated with unknown relative heights, but they are assumed to be bounded within the range $[0.05, 1]$. The intrinsic parameters of camera are: $m_0 = 320$ pixels, $n_0 = 240$ pixels, $\alpha_m = \alpha_n = 616$ pixels. The desired formation is specified by relative positions between leader–follower pairs. The desired relative position vectors for $R_1 - R_2$, $R_2 - R_4$, $R_1 - R_3$, $R_3 - R_5$ are, respectively, set as $r_{12}^d = r_{24}^d = [0.8, -0.2]^T, r_{13}^d = r_{35}^d = [0.8, 0.2]^T$, and the corresponding desired normalized coordinates for each follower robot are $(p_2^*, q_2^*) = (0.25, -0.34)$, $(p_3^*, q_3^*) = (-0.25, -0.34)$, $(p_4^*, q_4^*) = (0.25, 0.34)$, $(p_5^*, q_5^*) = (-0.25, 0.34)$. The linear and angular velocities of the group leader robot R_1 are $v_l = 1$ and $\omega_l = 0$. The controller gain are chosen as $K_{1i} = \text{diag}(0.05, 0.08)$ and $K_{2i} = \text{diag}(0.005, 0.002)$, and the observer gains are given by $\gamma_i = 0.5$, where $i \in \{2, 3, 4, 5\}$. In the performance function, the maximum allowable steady-state error is set to $\rho_\infty = 0.0081$ (5 pixels), and the convergence rate is $l = 2$.

The simulation results corresponding to the proposed controller (25)–(27) are presented in Fig. 5. Fig. 5(a) shows the formation group trajectory in the plane, where the desired V-formation is achieved at about $t = 2$ s. From Fig. 5(b), it can be seen that the formation errors of all followers quickly approaching to zero. As shown in Fig. 5(c), though very coarse initial values are used, all estimations can be guaranteed to remain bounded. As shown in Fig. 5(d) and (e), all the normalized image feature errors not only converge quickly but also retain within the predefined performance bounds; thus, the camera field of view constraints are always met. Under the proposed control algorithm, the normalized feature errors achieve the satisfying steady-state performance with about 0.005 (3 pixels). The simulation results show the validity and good performance of our formation control algorithm with field of view constraints.

B. Experimental Results

In addition to the simulation study, we further test the proposed control method in a real-world experiment on the mobile robots developed in our Robotic Laboratory. As shown in Fig. 6, the entire experimental platform includes an OptiTrack system, the leader robot with a orange ball acting as feature point, and the follower robot with monocular camera. The OptiTrack motion capture system is utilized to obtain the ground truth information about the 2-D positions of the mobile robots with respect to a global coordinate frame. The ground station computer communicates with the OptiTrack motion capture system via WIFI to record the data obtained by the OptiTrack and illustrate the trajectories of the whole formation. The Intel Realsense D435 as a monocular camera is used to get only its RGB image, and the camera parameters are the same with that in simulation. The follower robot R_f detects the ball on the leader R_l by the classical hough circle detection algorithm. The image processing algorithm, and the adaptive formation control law are directly implemented on the Intel NUC mini PC onboard the follower robot R_f. The feedback control loop runs at a frequency of about 50 Hz. The proposed algorithm is implemented in the robot operating system kinetic, running on Ubuntu 16.04. In the experiments, the controller gains are chosen as $K_1 = \text{diag}(0.008, 0.003)$ and $K_2 = \text{diag}(0.023, 0.010)$, and the observer gain is given by $\gamma = 0.5$. Consider the following two cases.

Case 1: Follower R_f follows a static leader R_l.

Case 2: Follower R_f follows R_l with circular motion.

In the first case, the desired normalized coordinates $(p^*, q^*) = (0.0, -0.3)$ for specifying the formation pattern is obtained when $r_{lf} = [0.9, 0.0]^{\mathrm{T}}$. In addition, the maximum allowable steady-state error is set to $\rho_\infty = 0.0162$ (10 pixels), and the decrement rate is set as $l = 0.3$ to perform the exponential convergence determined by $e^{-0.3t}$. Under this setting, the corresponding experimental results are given in Fig. 7. Fig. 7(a) illustrates the trajectories of the leader–follower robots recorded by the OptiTrack system, where the pentagon denotes the desired or the target position for the follower robot. Fig. 7(b) shows the input linear and angular velocities of follower robot according to the proposed controller. Fig. 7(c) and (d) shows the feature coordinate errors and the corresponding imposed performance bounds. It can be seen that the formation errors converge with

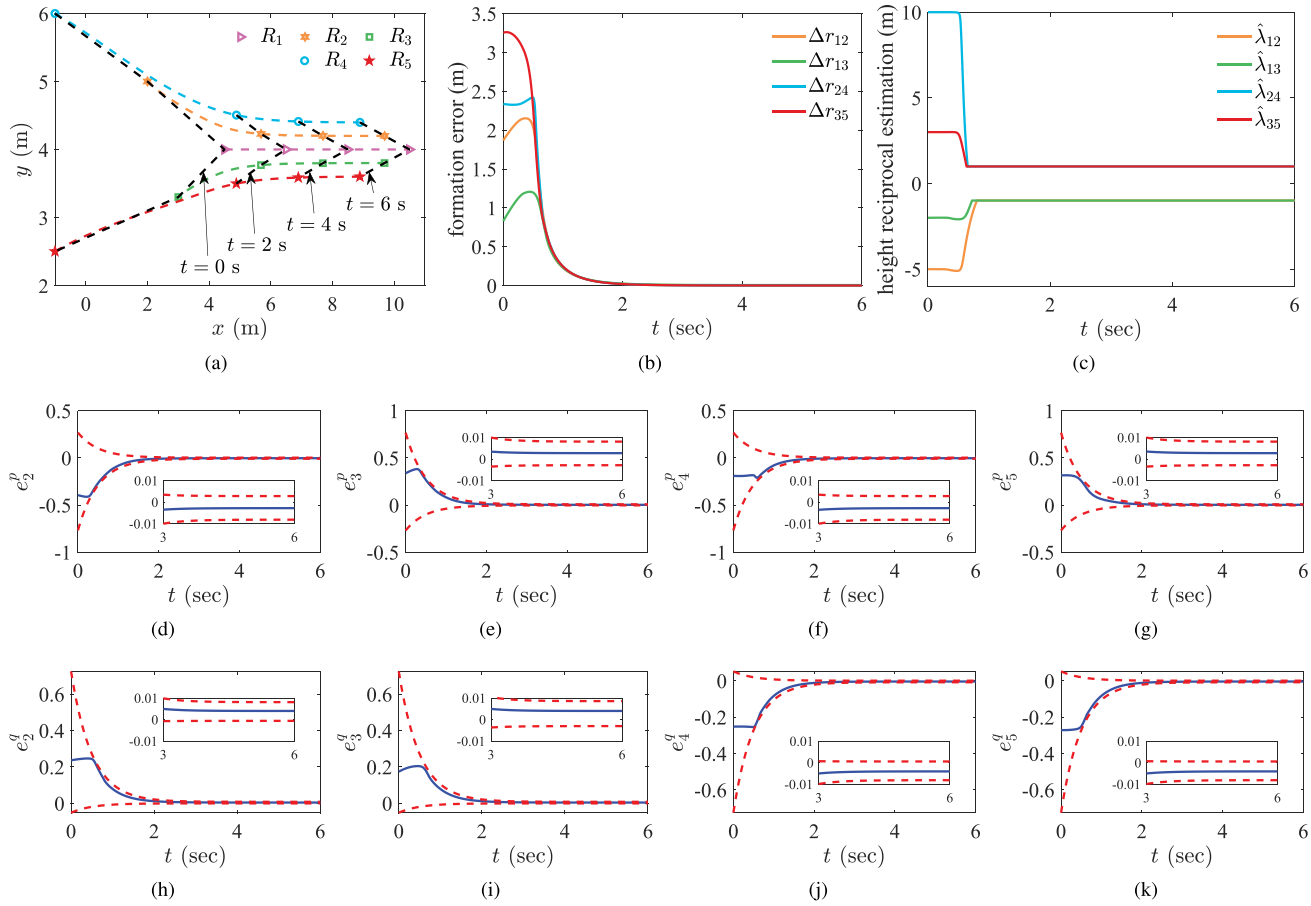

Fig. 5. Simulation results for the proposed controller. (a) Trajectories for whole formation process, where snapshots of robot positions are provided at every two seconds. (b) Formation error $\Delta r_{ij} = ||r_{ij} - r_{ij}^d||$, where r_{ij} and r_{ij}^d are, respectively, the actual and desired relative positions between leader robot R_i and follower robot R_j. (c) Estimation of the parameter $\lambda_{ij} = 1/h_{ij}$, where h_{ij} is the relative hight between the camera onboard the robot R_i and feature point attached to the follower R_j. (d)–(k) Evolution of the normalized image coordinate errors (blue) along with the corresponding applied performance bounds (red), where e_i^p and e_i^q denote, respectively, the first and the second coordinate errors of each follower robot i.

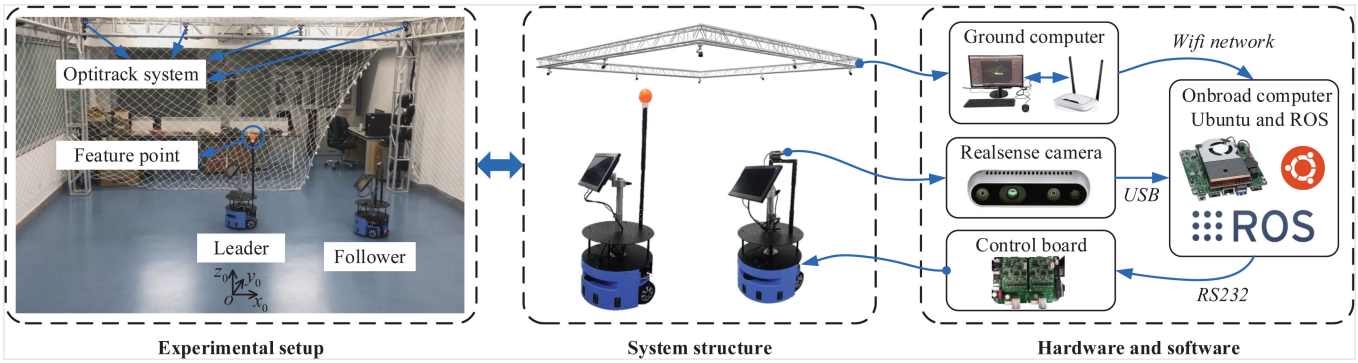

Fig. 6. Experimental setup for the vision-based leader–follower formation system.

satisfactory accuracy range about 0.0129 (8 pixels). The results show the good stability and performance of the control scheme for formation stabilization.

In the second case, the linear and angular velocities of the leader robot, respectively, are given as $v_f = 0.2$ and $w_f = 0.1$. Similarly, the desired normalized coordinates $(p^*, q^*) = (-0.3, -0.3)$ for specifying the formation pattern is obtained when $r_{lf} = [0.9, 0.27]^{\mathrm{T}}$. The parameters of the performance function are set as $\rho_\infty = 0.02435$ (15 pixels), $l = 0.1$. All the other parameters are chosen as the same with that in Case 1. The experimental results for the second case are given in Fig. 8. Fig. 8(a) shows the trajectories of the leader–follower robots,

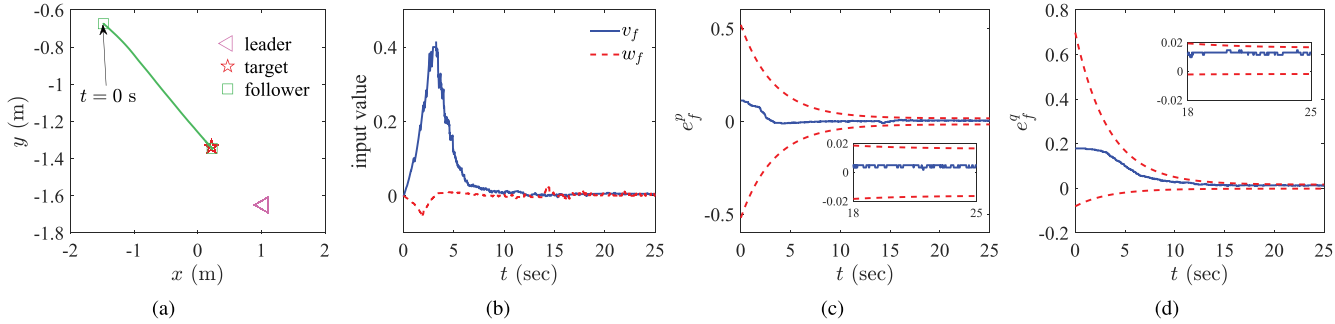

Fig. 7. Experimental results for the first case. (a) Trajectories for whole formation process, where the solid line illustrates the trajectory of the follower, the star marks the desired position for the follower, and the triangle represents the fixed position of the leader. (b) Linear and angular velocities of follower robot. (c) and (d) Evolution of the first and the second coordinate errors in normalized image plane (blue) along with the corresponding applied performance bounds (red).

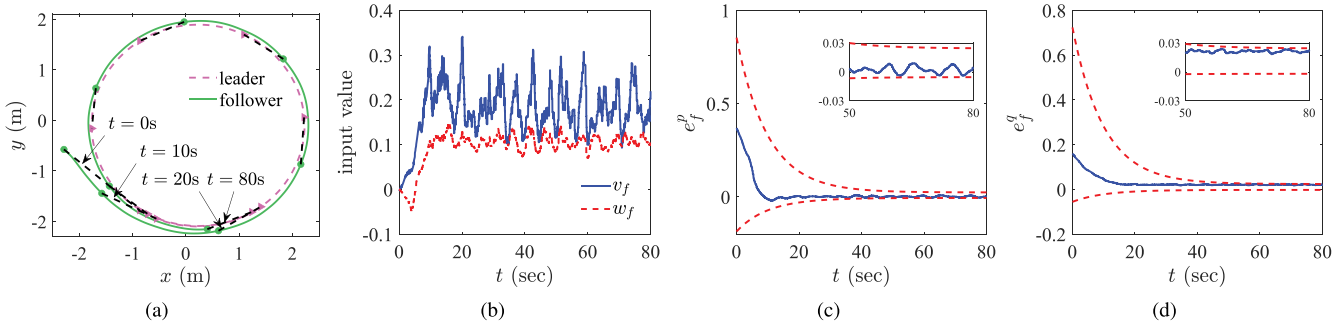

Fig. 8. Experimental results for the second case. (a) Trajectories for whole formation process, where snapshots of robot positions are provided at every ten seconds, and the leader and the follower are linked by dotted black line. (b) Linear and angular velocities of follower robot. (c) and (d) Evolution of the first and the second coordinate errors in normalized image plane (blue) along with the corresponding applied performance bounds (red).

where the circle and the square marks indicate, respectively, the position of the leader and the follower at the same moment. The linear and angular velocities of the follower with the proposed controller are depicted in Fig. 8(b). From Fig. 8(c) and (d), it can be observed that the feature errors are always guaranteed within the predefined performance bounds, and they converge to a predefined performance range about 0.023 (14 pixels). The results indicate that the proposed control algorithm still has a good performance in the case of formation tracking with a moving leader.

V. Conclusion

An adaptive visual feedback controller based on the prescribed performance control methodology was proposed to handle the visibility constraints inherently in the vision-based formation control problem. Different from most solutions that use distance and angle to maintain visibility, the proposed controller set performance specifications directly on normalized image coordinates to ensure visibility constraints, dynamic, and the steady-state performance. The developed control scheme was simple and effective, since it required less information, it does not need to measure or estimate the relative pose or velocity between robots. It can be implemented in the absence of GPS and WIFI signals, which greatly expands the applicability of our solution. In this article, we not only proved the global stability of the proposed algorithm with Lyapunov tools, but also verified its effectiveness by simulation and experiments. Future work is to extend the proposed strategy for robot formations in more complex real-world environments. Some practical issues, such as collision and obstacle avoidance need to be addressed in further studies. It is also interesting to investigate the cases where the observed features are occludes and the feature images are temporarily lost.

References

[1] M. Corah, C. OMeadhra, K. Goel, and N. Michael, "Communication-efficient planning and mapping for multi-robot exploration in large environments," *IEEE Robot. Autom. Lett.*, vol. 4, no. 2, pp. 1715–1721, Apr. 2019.

[2] J. Lopez, D. Perez, E. Paz, and A. Santana, "WatchBot: A building maintenance and surveillance system based on autonomous robots," *Robot. Auton. Syst.*, vol. 61, no. 12, pp. 1559–1571, 2013.

[3] L. Paull, M. Seto, J. J. Leonard, and H. Li, "Probabilistic cooperative mobile robot area coverage and its application to autonomous seabed mapping," *Int. J. Robot. Res.*, vol. 37, no. 1, pp. 21–45, 2018.

[4] J. Alonso-Mora, S. Baker, and D. Rus, "Multi-robot formation control and object transport in dynamic environments via constrained optimization," *Int. J. Robot. Res.*, vol. 36, no. 9, pp. 1000–1021, 2017.

[5] H. G. Tanner, G. J. Pappas, and V. Kumar, "Leader-to-formation stability," *IEEE Trans. Robot. Autom.*, vol. 20, no. 3, pp. 443–455, Jun. 2004.

[6] J. Shao, G. Xie, and L. Wang, "Leader-following formation control of multiple mobile vehicles," *IET Control Theory Appl.*, vol. 1, no. 2, pp. 545–552, 2007.
[7] L. Consolini, F. Morbidi, D. Prattichizzo, and M. Tosques, "Leader-follower formation control of nonholonomic mobile robots with input constraints," *Automatica*, vol. 44, no. 5, pp. 1343–1349, 2008.
[8] Z. Qiu, L. Xie, and Y. Hong, "Quantized leaderless and leader-following consensus of high-order multi-agent systems with limited data rate," *IEEE Trans. Autom. Control*, vol. 61, no. 9, pp. 2432–2447, Sep. 2016.
[9] X. Yu and L. Liu, "Distributed formation control of nonholonomic vehicles subject to velocity constraints," *IEEE Trans. Ind. Electron.*, vol. 63, no. 2, pp. 1289–1298, Feb. 2016.
[10] Z. Miao, Y.-H. Liu, Y. Wang, G. Yi, and R. Fierro, "Distributed estimation and control for leader-following formations of nonholonomic mobile robots," *IEEE Trans. Autom. Sci. Eng.*, vol. 15, no. 4, pp. 1946–1954, Oct. 2018.
[11] T. Balch and R. C. Arkin, "Behavior-based formation control for multi-robot teams," *IEEE Trans. Robot. Autom.*, vol. 14, no. 6, pp. 926–939, Dec. 1998.
[12] F. Arrichiello, S. Chiaverini, G. Indiveri, and P. Pedone, "The null space based behavioral control for non-holonomic mobile robots with actuators velocity saturation," *Int. J. Robot. Res.*, vol. 29, no. 10, pp. 1317–1337, 2010.
[13] M. A. Lewis and K. H. Tan, "High precision formation control of mobile robots using virtual structures," *Auton. Robot.*, vol. 4, no. 4, pp. 387–403, 1997.
[14] Q. Zhang, L. Lapierre, and X. Xiang, "Distributed control of coordinated path tracking for networked nonholonomic mobile vehicles," *IEEE Trans. Ind. Informat.*, vol. 9, no. 1, pp. 472–484, Feb. 2013.
[15] H. Rezaee and F. Abdollahi, "A decentralized cooperative control scheme with obstacle avoidance for a team of mobile robots," *IEEE Trans. Ind. Electron.*, vol. 61, no. 1, pp. 347–354, Jan. 2014.
[16] W. B. Dunbar and R. M. Murray, "Distributed receding horizon control for multi-vehicle formation stabilization," *Automatica*, vol. 42, no. 4, pp. 549–558, 2006.
[17] P. Wang and B. Ding, "Distributed RHC for tracking and formation of nonholonomic multi-vehicle systems," *IEEE Trans. Autom. Control*, vol. 59, no. 6, pp. 1439–1453, Jun. 2014.
[18] H. Fukushima, K. Kon, and F. Matsuno, "Model predictive formation control using branch-and-bound compatible with collision avoidance problems," *IEEE Trans. Robot.*, vol. 29, no. 5, pp. 1308–1317, Oct. 2013.
[19] H. Xiao, Z. Li, and C. L. P. Chen, "Formation control of leader-follower mobile robots' systems using model predictive control based on neural-dynamic optimization," *IEEE Trans. Ind. Electron.*, vol. 63, no. 9, pp. 5752–5762, Sep. 2016.
[20] H. Xiao and C. L. P. Chen, "Incremental updating multirobot formation using nonlinear model predictive control method with general projection neural network," *IEEE Trans. Ind. Electron.*, vol. 66, no. 6, pp. 4502–4512, Jun. 2019.
[21] K. K. Oh, M. C. Park, and H. S. Ahn, "A survey of multi-agent formation control," *Automatica*, vol. 53, pp. 424–440, 2015.
[22] R. Tron, J. Thomas, G. Loianno, K. Daniilidis, and V. Kumar, "A distributed optimization framework for localization and formation control: Applications to vision-based measurements," *IEEE Control Syst. Mag.*, vol. 36, no. 4, pp. 22–44, Aug. 2016.
[23] A. K. Das, R. Fierro, V. Kumar, J. P. Ostrowski, J. Spletzer, and C. J. Taylor, "A vision-based formation control framework," *IEEE Trans. Robot. Autom.*, vol. 18, no. 5, pp. 813–825, Oct. 2002.
[24] M. Chueh, Y. L. W. Au Yeun, K. P. C. Lei, and S. S. Joshi, "Following controller for autonomous mobile robots using behavioral cues," *IEEE Trans. Ind. Electron.*, vol. 55, no. 8, pp. 3124–3132, Aug. 2008.
[25] G. L. Mariottini *et al.*, "Vision-based localization for leader-follower formation control," *IEEE Trans. Robot.*, vol. 25, no. 6, pp. 1431–1438, Dec. 2009.
[26] F. Morbidi, G. L. Mariottini, and D. Prattichizzo, "Observer design via immersion and invariance for vision-based leader-follower formation control," *Automatica*, vol. 46, no. 1, pp. 148–154, 2010.
[27] A. P. Dani, N. Gans, and W. E. Dixon, "Position-based visual servo control of leader-follower formation using image-based relative pose and relative velocity estimation," in *Proc. IEEE Amer. Control Conf.*, 2009, pp. 5271–5276.
[28] H. Poonawala, A. C. Satici, N. Gans, and M. W. Spong, "Formation control of wheeled robots with vision-based position measurement," in *Proc. IEEE Amer. Control Conf.*, 2012, pp. 3173–3178.
[29] B. Fidan, V. Gazi, S. Zhai, N. Cen, and E. Karatas, "Single-view distance-estimation-based formation control of robotic swarms," *IEEE Trans. Ind. Electron.*, vol. 60, no. 12, pp. 5781–5791, Dec. 2013.
[30] X. Liang, Y.-H. Liu, H. Wang, W. Chen, K. Xing, and T. Liu, "Leader-following formation tracking control of mobile robots without direct position measurements," *IEEE Trans. Autom. Control*, vol. 61, no. 12, pp. 4131–4137, Dec. 2016.
[31] R. Vidal, O. Shakernia, and S. Sastry, "Following the flock: distributed formation control with omnidirectional vision-based motion segmentation and visual servoing," *IEEE Robot. Autom. Mag.*, vol. 11, no. 4, pp. 14–20, Jan. 2004.
[32] X. Chen and Y. Jia, "Adaptive leader-follower formation control of non-holonomic mobile robots using active vision," *IET Control Theory Appl.*, vol. 9, no. 8, pp. 1302–1311, 2015.
[33] H. Wang, D. Guo, X. Liang, W. Dong, G. Hu, and K. K. Leang, "Adaptive vision-based leader-follower formation control of mobile robots," *IEEE Trans. Ind. Electron.*, vol. 64, no. 4, pp. 2893–2902, Apr. 2017.
[34] X. Liang, H. Wang, Y.-H. Liu, W. Chen, and T. Liu, "Formation control of nonholonomic mobile robots without position and velocity measurements," *IEEE Trans. Robot.*, vol. 34, no. 2, pp. 434–446, Apr. 2018.
[35] F. Morbidi, F. Bullo, and D. Prattichizzo, "Visibility maintenance via controlled invariance for leader-follower vehicle formations," *Automatica*, vol. 47, no. 5, pp. 1060–1067, 2011.
[36] D. Panagou and V. Kumar, "Cooperative visibility maintenance for leader-follower formations in obstacle environments," *IEEE Trans. Robot.*, vol. 30, no. 4, pp. 831–844, Aug. 2014.
[37] X. Liu, S. S. Ge, and C. H. Goh, "Vision-based leader-follower formation control of multiagents with visibility constraints," *IEEE Trans. Control Syst. Technol.*, vol. 27, no. 3, pp. 1326–1333, May 2019.
[38] C. K. Verginis, C. P. Bechlioulis, D. V. Dimarogonas, and K. J. Kyriakopoulos, "Decentralized 2-d control of vehicular platoons under limited visual feedback," in *Proc. IEEE/RSJ Int. Conf. Intell. Robot. Syst.*, 2015, pp. 3566–3571.
[39] C. P. Bechlioulis, S. Heshmati-alamdari, G. C. Karras, and K. J. Kyriakopoulos, "Robust image-based visual servoing with prescribed performance under field of view constraints," *IEEE Trans. Robot.*, vol. 35, no. 4, pp. 1063–1070, Aug. 2019.
[40] J. Na, Q. Chen, X. Ren, and Y. Guo, "Adaptive prescribed performance motion control of servo mechanisms with friction compensation," *IEEE Trans. Ind. Electron.*, vol. 61, no. 1, pp. 486–494, Jan. 2014.
[41] S. L. Dai, S. He, H. Lin, and C. Wang, "Platoon formation control with prescribed performance guarantees for USVs," *IEEE Trans. Ind. Electron.*, vol. 65, no. 5, pp. 4237–4246, May 2018.
[42] K. Lu, Z. Liu, G. Lai, C. L. P. Chen, aand Y. Zhang, "Adaptive consensus tracking control of uncertain nonlinear multiagent systems with predefined accuracy," *IEEE Trans. Cybern.*, to be published.

Jie Lin received the B.S. degree in automation from the College of Electrical Engineering and Automation, Fuzhou University, Fujian, China, in 2019. He is currently working toward the Ph.D. degree in control science and engineering with the Hunan University, Changsha, China.

His current research interests include multi-robot systems, visual servoing, and nonlinear control.

Zhiqiang Miao (Member, IEEE) received the B.S. and Ph.D. degrees in electrical and information engineering from Hunan University, Changsha, China, in 2010 and 2016, respectively.

From 2014 to 2015, he was a Visiting Scholar with the University of New Mexico, Albuquerque, NM, USA. From 2016 to 2018, he was a Postdoctoral Fellow with the Department of Mechanical and Automation Engineering, The Chinese University of Hong Kong, Hong Kong. He is currently an Associate Professor with the College of Electrical and Information Engineering, Hunan University. His current research interests include multirobot systems, visual servoing, motion planning, and nonlinear control.

Hang Zhong received the B.S., M.S., and Ph.D. degrees in automation science from the College of Electrical and Information Engineering, Hunan University, Changsha, China, in 2013, 2016, and 2020, respectively.

He is currently a Postdoctoral Fellow. His current research interests include robotics modeling and control, visual servo control, and path planning of the aerial robots.

Weixing Peng received the B.S. degree in automation science from the College of Information Science and Technology, Donghua University, Shanghai, China, in 2016. He is currently working toward the Ph.D. degree in control theory and control engineering with Hunan University, Changsha, China.

His current research interests include vision servo control, viewpoint planning, and 3-D reconstruction of autonomous measurement robot technology for engine blade.

Yaonan Wang received the B.S. degree in computer engineering from East China Science and Technology University (ECSTU), Fuzhou, China, in 1981, and the M.S. and Ph.D. degrees in electrical engineering from Hunan University, Changsha, China, in 1990 and 1994, respectively.

From 1994 to 1995, he was a Postdoctoral Research Fellow with the National University of Defence Technology, Changsha. From 1981 to 1994, he was with ECSTU. From 1998 to 2000, he was a Senior Humboldt Fellow in Germany. From 2001 to 2004, he was a Visiting Professor with the University of Bremen, Bremen, Germany. He has been a Professor with Hunan University since 1995. His current research interests include robotics, intelligent perception and control, and computer vision for industrial applications.

Prof. Wang is an Academician of the Chinese Academy of Engineering.

Rafael Fierro (Senior Member, IEEE) received the M.Sc. degree in control engineering from the University of Bradford, Bradford, U.K., in 1990 and the Ph.D. degree in electrical engineering from the University of Texas at Arlington, Arlington, TX, USA, in 1997.

He held a Postdoctoral appointment with the GRASP Laboratory, University of Pennsylvania, Philadelphia, PA, USA, and a faculty position with the Department of Electrical and Computer Engineering, Oklahoma State University, Stillwater, OK, USA. Since 2007, he has been a Professor with the Department of Electrical and Computer Engineering, University of New Mexico, Albuquerque, NM, USA, where he directs the Multiagent, Robotics, Hybrid and Embedded Systems Laboratory. His current research interests include hybrid and embedded systems, heterogeneous multivehicle coordination, cooperative and distributed control of multiagent systems, mobile sensor networks, and robotics.

Dr. Fierro was a recipient of the Fulbright Scholarship, the 2004 National Science Foundation CAREER Award, and the 2007 International Society of Automation Transactions Best Paper Award. He is an Associate Editor for the IEEE TRANSACTIONS ON AUTOMATION SCIENCE AND ENGINEERING.